# Electrorotation of colloidal particles in liquid crystals

G. Liao, I. I. Smalyukh, J. R. Kelly, O. D. Lavrentovich, and A. Jákli
*Liquid Crystal Institute and Chemical Physics Interdisciplinary Program, Kent State University, Kent, Ohio 44242, USA*
(Received 25 February 2005; published 13 September 2005; corrected 19 September 2005)

We present the first observations of dc electric-field-induced rotational motion of finite particles in liquid crystals. We show that the electrorotation is essentially identical to the well-known Quincke rotation, which in liquid crystals triggers an additional translational motion at higher fields. In the smectic phase the translational motion is confined to the two-dimensional geometry of smectic layers, in contrast to the isotropic and nematic phases, where the particles can move in all three dimensions. We demonstrate that by a proper analysis of the electrorotation, one can determine the in-plane viscosity of smectic liquid crystals. This method needs only a small amount of material, does not require uniform alignment over large areas, and enables probing rheological properties locally.

DOI: 10.1103/PhysRevE.72.031704 PACS number(s): 61.30.−v, 77.84.Nh, 83.80.Xz

Electrophoresis, i.e., electrically induced rotational and translational motion of small particles in fluids, is an ancient, but still active science [1]. Most electrophoretic motions are allowed by symmetry (e.g., along the field), however, some motions require symmetry-breaking transitions, and appear only above a threshold electric field. An example of the latter is a dc electric-field-induced steady rotation of solid spherical objects that, in isotropic liquids, was observed first in 1893 by Weiler [2] (Quincke rotation [3]), but was explained only in 1984 by Jones [4]. Another interesting example is an induced translational motion normal to the electric field. This has been observed only for long, slender particles whose charges vary along their contour [5] and was explained in terms of coupling between surface charge and shape modulation [6]. Electrophoretic studies in liquid crystals are scarce [7] and are limited to motions of nanoparticles in lyotropic liquid crystals that do not require symmetry-breaking transitions. It is clear, however, that the techniques based on one-bead microrheology [8] developed recently to monitor the mechanical properties of viscoelastic soft materials [9], might be extremely helpful in analyzing rheological properties of smectic liquid crystal materials, which can be considered as stacks of two-dimensional fluid layers. Study of the complex hydrodynamics of smectic liquid crystals by the traditional shear flow experiments [10,11] is very difficult, because of the generation of defects and macroscopic flows. In this Letter we report the first observations of electrorotation and electrotranslation of microscopic cylindrical and spherical inclusions dispersed in smectic materials. We show that a quantitative analysis of the electrorotation can be used to determine the in-plane viscosity of the smectic liquid crystals.

We have studied two commercially available liquid crystalline (LC) materials: octyl cyano biphenyl (8CB) from Aldrich, and a mixture CS 2003 from Chisso, Inc. 8CB has a smectic-*A* (Sm*A*) phase in temperature range 23 °C–33 °C characterized by a large positive dielectric anisotropy ($\Delta\varepsilon=8$ at 32 °C). CS2003 is a room temperature ferroelectric Sm$C^*$ mixture with ferroelectric polarization $P_0 \sim 40$ nC/cm$^2$ and negative dielectric anisotropy ($\Delta\varepsilon=-0.6$ at 50 °C). It also has a Sm$A^*$ phase between 56 °C and 64 °C, and a chiral nematic ($N^*$) phase between 64 °C and 90 °C. For fluorescence confocal polarizing microscopy (FCPM) observations, the LCs were doped with ~0.01% of fluorescent dye BTBP [*N*,*N*′-bis(2,5-di-tert-butylphenyl)-3,4,9,10-perylenedicarboximide] [12]. Glass spheres (beads) of 4.5 $\mu$m diameter and cylinders of 4.5 $\mu$m and 10 $\mu$m diameters with length/diameter ratios varying between 1 and 10, were dispersed at low concentrations in LC films of thicknesses in the range of 6–30 $\mu$m. We investigated films with uniform thickness (uniformity is ±0.5 $\mu$m over 1 cm$^2$) and wedge-shape cells (wedge angles ~20 $\mu$m/1 cm). The observations were carried out by polarizing microscopy (Olympus BX60), and by a fast version of FCPM based on a scanning CARV® system with a spinning Nipkow disk integrated with a Nikon microscope (Eclipse E-600) that enabled taking motion pictures of the textures. The electric field was applied normal to the film surfaces via a potential difference between transparent indium tin oxide (ITO) layers deposited on the glass plates of the cells. The ITO layers were coated with a polyimide (PI2555 from HD Micro Systems) film rubbed unidirectionally to promote director alignment parallel to the rubbing direction.

Far from the dispersed particles such a surface treatment produced uniform bookshelf layer structure (layers are normal to the substrates). In case of CS2003 ($\Delta\varepsilon<0$) this alignment remained stable in electric fields applied across the substrates. In case of 8CB ($\Delta\varepsilon>0$), a sufficiently strong field realigns the layers from their original bookshelf vertical orientation. In the transition range (2.5 V/$\mu$m$<E<$4 V/$\mu$m), the layers are tilted with numerous defects. At $E>4$ V/$\mu$m a fairly uniform homeotropic configuration forms, i.e., the smectic layers are parallel to the substrates. If the field is switched off, the resulting texture depends on the preapplied field: if it is smaller than 7 V/$\mu$m, the bookshelf structure gradually restores itself; however, if the field is larger than 7 V/$\mu$m, the surface anchoring is broken and the homeotropic texture is preserved at the zero electric field as a metastable state.

In the bookshelf textures at zero electric fields, most of the *glass cylinders* are aligned parallel to the rubbing direction, i.e., along the director. FCPM textures of the vertical

 

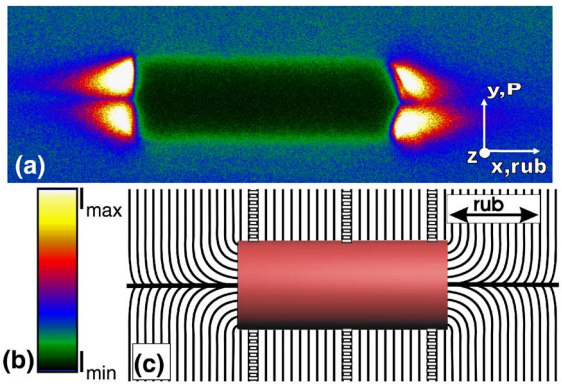


FIG. 1. (Color online) (a): In-plane FCPM texture of a 4.5 $\mu$m cylinder; (b) the FCPM color-coded intensity scale; (c) the reconstructed director and layer structure that has rotational symmetry with respect to the cylinder axis.

cross sections of the 8CB samples, Fig. 1(a), show that the director is parallel to the cylinder surface everywhere; two toric focal conic domains [13] cup the ends of the cylinder.

When the dc field exceeds the threshold $E_r$, the cylinders start to rotate about their symmetry axes. The rotation of the cylinders is easily observable under the microscope, as the edges of the cylinders are often slanted. Both the threshold field, $E_r$, and the angular frequency of rotation, $\omega(E)$, could be measured by recording the rotation and tracking the frames. The electric field dependence of the angular velocity for CS2003 at 59 °C (Sm*A* phase) and at 50 °C (Sm$C^*$ phase) are plotted in Fig. 2(a). The threshold $E_r$ was observed rapidly increasing at decreasing temperatures (0.34 V/$\mu$m at 59 °C and 2.1 V/$\mu$m at 50 °C), however, the slopes of the curves at field much higher than the threshold only slightly depend on the temperature. The determination of the threshold is not precise (~10% error), because the onset varies slightly from particle to particle, and some of the particles oscillate back and forth near the threshold. Within the measurement error cylinders with different radii rotate with the same angular velocity. The rotation velocity is basically independent of the length of the cylinders if the length/diameter ratio is larger than about 5. Shallow cylinders rotate significantly more slowly, because the defects near the edges become more important.

Similar angular velocity values could be measured at around three times smaller fields in 8CB at 32 °C (for example, at 2.5 V/$\mu$m $\omega \sim 30\ s^{-1}$), although there, the data scatter much more due to the field-induced layer realignment.

Electrorotations with lower thresholds were also observed in the nematic, and in the isotropic phases of both materials, indicating that the effect does not require anisotropy, similar to the classical Quincke rotation [3], which only require that the charge relaxation time of the inclusion ($\tau_s = \varepsilon_s/\sigma_s$) be larger than the charge relaxation time of the liquid matrix ($\tau_l = \varepsilon_l/\sigma_l$).

This is easily satisfied for liquid crystals ($\tau_s > \tau_{lc}$), because the conductivity of the glass particles ($\sigma_s < 10^{-12}$ S m$^{-1}$) is much smaller than that of the liquid crystals ($\sigma_{lc} = 0.9 \times 10^{-9}$ S/m for CS2003, and

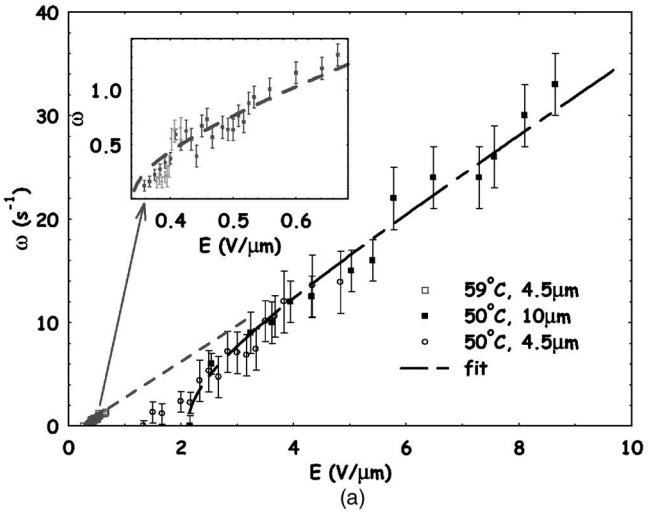


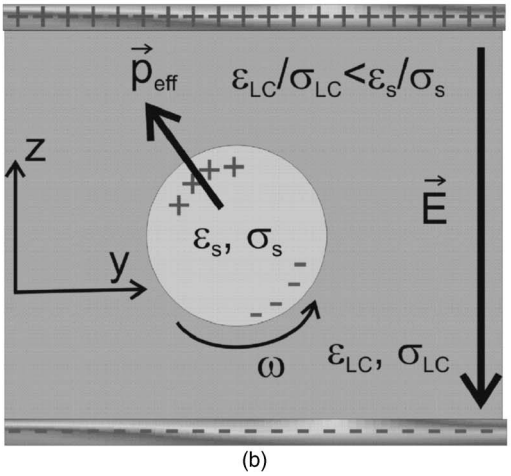


FIG. 2. (a) The measured electric field dependence of the angular frequency of 4.5 and 10 $\mu$m diameter cylinders embedded in a 12 $\mu$m thick CS2003 sample at 50 °C and 59 °C. Dashed lines are fits using Eq. (4) with viscosities $\eta$=5.5 Pa s and $\eta$=0.9 Pa s, respectively. (b) An illustration of the proposed physical mechanism [4] leading to the electrorotation.

$\sigma_{lc} \sim 0.7 \times 10^{-9}$ S/m for 8CB), whereas the relative dielectric constants are comparable [$\varepsilon_s$=3.9, $\varepsilon_{\parallel}$(8CB)=14, $\varepsilon_{\perp}$(8CB)=6, $\varepsilon_{\parallel}$(CS2003)=3, $\varepsilon_{\perp}$(CS2003)=3.6]. In such a case, the distribution of free charges on the inclusion's surface is such that they are repelled from the electrodes (i.e., the negative charge on the cylindrical surface is close to the negative electrode, Fig. 2(b). This situation is unstable against small rotational perturbations, and the solid inclusion will rotate around the axis perpendicular to the applied field, as observed in the experiment. Although the theoretical description of the Quincke rotation for the case of spheres in isotropic fluids cannot be directly adopted for describing cylinders rotating in the liquid crystals, the underlying physics is similar. Neglecting edge effects, the rotation of slender cylinders involves a two-dimensional flow; consequently, we need a 2-D model. Such a model was worked out by Feng [14] and provides a formula for the threshold electric field $E_r$, given as

$$E_r^2 = \alpha\eta[(1+S)(1+R)]/[\varepsilon_l(1-\tau_l/\tau_s)\tau_{MW}]. \quad (1)$$

This expression is valid both for spheres and slender cylinders; only the parameters are different. For spheres [15] $\alpha=4/3$, $S=2\varepsilon_l/\varepsilon_s$, $R=\sigma_s/2\sigma_l$, and $\tau_{MW}=(\varepsilon_s+2\varepsilon_l)/(\sigma_s+2\sigma_l)$, whereas for slender cylinders [14] $\alpha=1$, $S=\varepsilon_l/\varepsilon_s$, $R=\sigma_s/\sigma_l$, and $\tau_{MW}=(\varepsilon_s+\varepsilon_l)/(\sigma_s+\sigma_l)$. In these expressions $\varepsilon_l$, $\sigma_l(\varepsilon_s,\sigma_s)$ are the dielectric constant and electrical conductivity of the liquid (solid), respectively, $\tau_{MW}$ is the Maxwell-Wagner interfacial polarization relaxation time, and $\eta$ is the viscosity.

For both spheres and cylinders, the angular velocity as a function of the applied field can be given as

$$\omega = \frac{1}{\tau_{MW}}\sqrt{\frac{E^2}{E_r^2}-1}. \quad (2)$$

In case of our slender cylinder-liquid crystal system, where $\sigma_{lc} \gg \sigma_s$ and $\varepsilon_{lc} \sim \varepsilon_s$, the expression for the threshold electric field simplifies to

$$E_r^2 = \eta\frac{\sigma_{lc}}{\varepsilon_o^2\varepsilon_{lc}\varepsilon_s}, \quad (3)$$

where the relevant viscosity corresponds to the Miesovitz component $\eta_a$, because the shear plane is perpendicular to the director [10]. From the measured threshold field, additional electrical conductivity and the dielectric constants data one can get the viscosity from Eq. (3). With the parameters of CS2003 at 50 °C listed above, we get $\eta=6$ Pa s, whereas in case of 8CB at 32 °C we obtain only $\eta \sim 1$ Pa s.

Actually, we can determine the viscosity, even without the need for measuring the conductivity and the dielectric constant of the LC, by measuring both $E_r$ and $\omega$, and combining Eqs. (2) and (3), giving

$$\omega(E) = \frac{E_r^2\varepsilon_s\varepsilon_o}{\eta(1+\varepsilon_s/\varepsilon_{lc})}\sqrt{\frac{E^2}{E_r^2}-1}. \quad (4)$$

For $E \gg E_r$, this further simplifies to $\omega(E)=E_r\varepsilon_s\varepsilon_0 E/\eta(1+\varepsilon_s/\varepsilon_{lc})$. In spite of the ambiguity in determining the angular velocity near the threshold, the electric field dependence of the measured angular frequency can be satisfactorily fitted by Eq. (4) [see Fig. 1(e) for CS2003 at 50 °C and 59 °C], giving $\eta_a=5.5$ Pa s and $\eta_a=0.9$ Pa s, at 50 °C and 59 °C, respectively. Electrorotation measurements for 8CB at 32 °C gave $E_r=0.6$ V/$\mu$m and $\omega(E\ E_r)/E \sim 12 \times 10^{-6}$ mV$^{-1}$ s$^{-1}$, which provide $\eta_a=1.6$ Pa s. These values are in fairly good agreement with the results obtained using conductivity and dielectric data, and only the threshold field measurement. We note that $\eta_a$ was already measured for 8CB, and it was found [16] to be ~1.5 Pa s at shear rates corresponding to the highest rates (50 s$^{-1}$) in our experiments. This agreement clearly indicates that electrorotation of cylindrical inclusions can be used to study the rheology of liquid crystals.

At further increasing fields, the rotating cylinders are set into translational motion at $E_{th} > E_r$. In the isotropic and nematic phases, the direction of the motion occurs in three dimensions; however, in the smectic phases the axes of the cylinders move strictly along the smectic layers, i.e., the motion is two dimensional. Due to the irregular shape of the edges of the cylinders, the speed of the motion is somewhat irregular. To obtain more reliable results from the field-induced translational motion we studied spherical beads instead of cylinders.

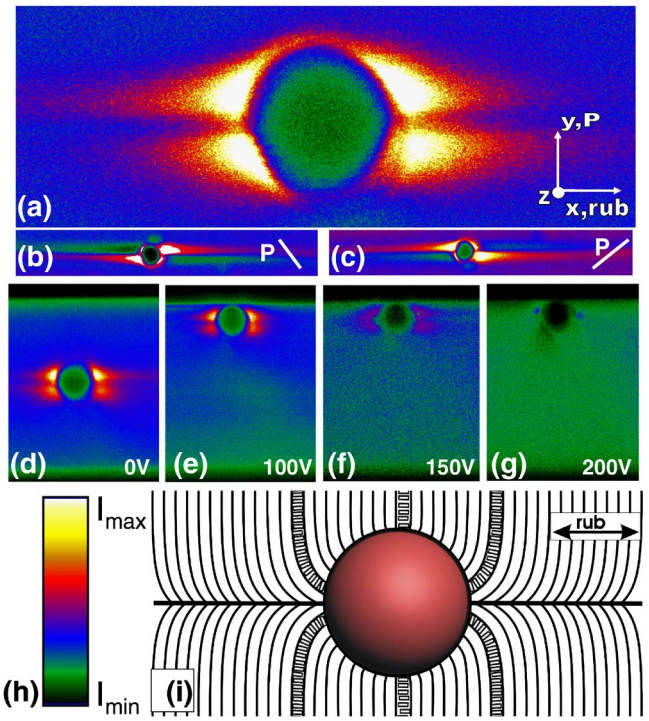


FIG. 3. (Color online) In-plane FCPM texture of the director distortions of 8CB at room temperature around a 4.5 $\mu$m spherical particle. (a)–(d). Far from the beads the liquid crystal is in bookshelf geometry (layers normal to substrates). A linear polarizer is orthogonal (a) and at about ±45 deg (b), (c) to the rubbing direction; (d) vertical FCPM cross section with the particle at rest close to the center of a 30 $\mu$m thick cell at a zero field. Note that the director distortions at the particle are similar to those in the in-plane section, indicating rotational symmetry around the defect line; (e)–(g) vertical FCPM cross sections indicating changes of particle positions and distortions in the director field around the spheres at different electric fields. The layers are distorted in (e), (f) and practically parallel to the substrates in (g); (h) the FCPM color-coded intensity scale; (i) reconstructed layers and director pattern around the particle embedded in the system of parallel smectic layers.

At zero electric fields in the bookshelf smectic layer alignment, the *spherical beads* are surrounded by two defect "wings" spanning along the layer normal (Fig. 3), similar to defect lines around isotropic droplets in Sm*A* liquid crystals of planar anchoring reported by Blanc and Kleman [17]. The length of the wings is about 30–100 $\mu$m in the Sm*A* phases of both 8CB and CS2003, whereas in the Sm$C^*$ structure the wings are much shorter (~5–10 $\mu$m), and sometimes are not even observable.

Although their electrorotation cannot be easily seen (they are too symmetric), careful observations revealed that they also spin around their axes normal to the field, with a threshold in reasonably good agreement with Eq. (1). Similar to the cylinders, the translational motions occur at threshold elec-

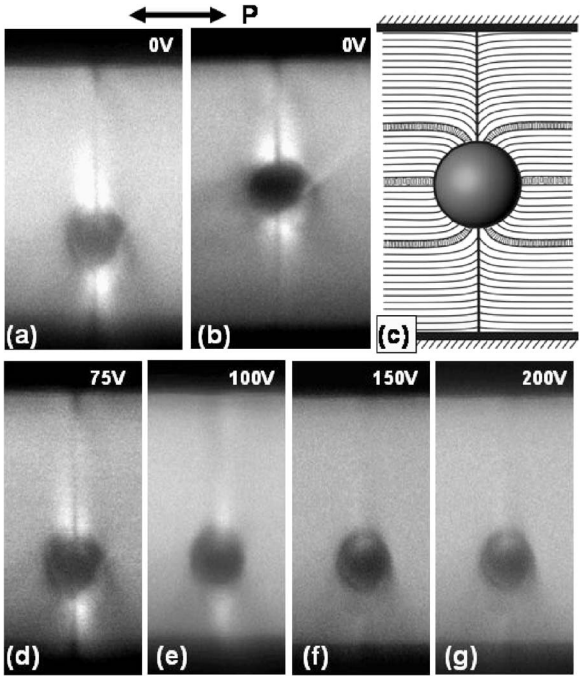


FIG. 4. Vertical FCPM textures of 8CB at room temperature in horizontal layer alignment. (a), (b) textures around a 4.5 $\mu$m glass bead right after the field has been turned off (a) and 10 minutes later (b); (c) the corresponding layer pattern around a sphere. The director structure has rotational symmetry around the vertical defect lines. (d)–(g) Textures around a bead under different electric fields: 3 V/$\mu$m (d), 4 V/$\mu$m (e), 6 V/$\mu$m (f) and 8 V/$\mu$m (g).

tric fields $E_{th}$, which is higher than $E_r$ ($E_{th} \sim 3.5$ V/$\mu$m for CS2003 at $T=50$ °C and $E_{th} \sim 2.5$ V/$\mu$m for 8CB at $T=32$ °C).

The translational motion takes place along the smectic layers and its direction does not depend on the direction of the gradient of the film thickness up to the wedge angle of $2 \times 10^{-3}$ rad. FCPM studies show that at zero fields the beads are evenly distributed between the substrates, but when the translational motion is induced, they eventually all end up at either the top or bottom of the film (Figs. 3(d)–3(g)), where they move along the substrates. When the fields are turned off the beads stick to the substrates and do not move back toward the inside of the film.

In the Sm*A* phase of the studied materials, there is a narrow range above $E_{th}$, where the particles travel by less than their diameter and bounce back after the field is turned off. This indicates elastic behavior, which is due to the layer distortions around the particles (see Fig. 3(i)). At higher fields the particles travel much farther than their diameter and only partially recoil after the field removal, indicating viscoelastic behavior. In this range the defect wings shrink and gradually vanish (Figs. 3(e)–3(g)). At fields higher than $E_v$ ($\sim 7$ V/$\mu$m for 8CB at $T=32$ °C and $\sim 6$ V/$\mu$m for CS2003 at 50 °C) the particles simply stop after field removal indicating a purely viscous response. In this range the speed of the translation is about 100 $\mu$m/s for the CS2003 and about 20 $\mu$m/s for 8CB.

In the films where the homeotropic texture remains stable after field removal, similar to the bookshelf alignment, defect lines form at the zero field, but now they span vertically normal to the cell substrates (see Figs. 4(a)–4(c)). In addition, some of the particles that were originally close to a substrate [Fig. 4(a)] gradually (in about 10 min) move toward the center of the cell [Fig. 4(b)], probably because the spheres at the surfaces lead to inclined smectic layers that cost surface anchoring energy [18]. When we apply electric fields in the horizontal layer alignment, the vertical defect lines gradually disappear, just as in the bookshelf alignment (see Figs. 4(d)–4(g)).

In summary, we have presented the first observations of dc electric-field-induced rotational and translational motion of finite particles in liquid crystals. We showed that the electric field-induced rotation is analogous to the Quincke rotation, and its proper analysis can be used to measure the viscosity coefficient $\eta_a$ of smectic liquid crystals. This is especially important, because this method does not require uniform alignment over centimeter ranges, and allows one to probe local viscous properties. We have also demonstrated the onset of a translational motion along the smectic layers. The details of the physical mechanism of the field-induced translational motion, and the defect disappearance mechanism will be the subject of future studies.

## ACKNOWLEDGMENT

Part of this work was financially supported by the NSF, Grant No. DMR-0315523.

[1] *Interfacial Electrokinetics and Electrophoresis*, edited by Á. V. Delgado (Marcel Dekker, Inc., New York, 2002).
[2] W. Weiler, Z. Phys. Chem. Unterricht, Heft IV, 194 (1893).
[3] G. Quincke, Ann. Phys. Chem. **11**, 27 (1896).
[4] T. B. Jones, IEEE Trans. Ind. Appl. **1A-20**, 845 (1984); and *Electromechanics of Particles* (Cambridge University Press, New York, 1995).
[5] Y. Solomentsev and J. L. Anderson, J. Fluid Mech. **279**, 197 (1994).
[6] D. Long and A. Ajdari, Phys. Rev. Lett. **81**, 1529 (1998).
[7] D. Mizuno, Y. Kimura, and R. Hayakawa, Phys. Rev. Lett. **87**, 088104-1 (2001); and Phys. Rev. E **70**, 011509 (2004).
[8] For a review see T. Gisler and D. A. Weitz, Curr. Opin. Colloid Interface Sci. **3**, 586 (1998); F. C. MacKintosh and C. F. Schmidt, *ibid.* **4**, 300 (1999).
[9] A. Palmer, T. G. Mason, J. Xu, S. C. Kuo, and D. Wirtz, Biophys. J. **76**, 1063 (1999).
[10] R. G. Horn and M. Kleman, Ann. Phys. (Paris) **3**, 229 (1978); S. Bhattacharya and S. V. Letcher, Phys. Rev. Lett. **44**, 414 (1980).
[11] R. G. Larson, *The Structure and Rheology of Complex Fluids* (Oxford University Press, Oxford, 1999).

[12] I. I. Smalyukh, S. V. Shiyanovskii, and O. D. Lavrentovich, Chem. Phys. Lett. **336**, 88 (2001).
[13] M. Kleman and O. D. Lavrentovich, *Soft Matter Physics: An Introduction* (Springer-Verlag, New York, 2003), p. 638.
[14] J. Q. Feng, J. Colloid Interface Sci. **246**, 112 (2002).
[15] S. Krause and P. Chandratreya, J. Colloid Interface Sci. **206**, 10 (1998).
[16] P. Panizza, P. Archambault, and D. Roux, J. Phys. II **5**, 303 (1995).
[17] C. Blanc and M. Kleman, Eur. Phys. J. E **4**, 241 (2001).
[18] Z. Li and O. D. Lavrentovich, Phys. Rev. Lett. **73**, 280 (1994).